ISSN 1068-3755, Surface Engineering and Applied Electrochemistry, 2017, Vol. 53, No. 3, pp. 265–273. © Allerton Press, Inc., 2017.

Sinapis alba as an Anti-Rusting Agent for Corrosion of Stainless Steel in Hydrochloric Acid Medium[1]

N. Shwetha and Padmalatha Rao*

Department of Chemistry, Manipal Institute of Technology, Manipal, Udupi, Karnataka

**e-mail: padmalatha.rao@manipal.edu*

Received July 29, 2016

Abstract—Protection against corrosion using *Sinapis alba* was studied for the corrosion control of stainless steel in 0.5 M HCl. The electrochemical techniques such as potentiodynamic polarization measurements and electrochemical impedance spectroscopy were used for the stainless steel protection studies. Surface morphology studies were done using scanning electron microscopy/energy dispersive X-ray analysis. Kinetic and thermodynamic parameters were evaluated and discussed. The mechanism for the corrosion inhibition was proposed. The obtained results showed that *Sinapis alba* acted as a mixed-type inhibitor, with the maximum inhibition efficiency of 88% for the concentration of 0.1 g L^{-1} at 323K. It was chemically adsorbed on stainless steel and obeyed the Langmuir adsorption isotherm. *Sinapis alba* emerged as an effective eco-friendly corrosion inhibitor for the corrosion control of stainless steel in the HCl acid medium. Surface morphology studies confirmed the adsorption of this inhibitor onto the surface of the metal. The results obtained via potentiodynamic polarisation and electrochemical impedance spectroscopy was in agreement with each other.

Keywords: stainless steel, green inhibitor, *Sinapis alba*, electrochemical measurements, scanning electron microscopy/energy dispersive X-ray analysis, adsorption

DOI: 10.3103/S1068375517030139

INTRODUCTION

Stainless steel is an alloy of iron, carbon and chromium. It has a wide range of applications in various fields such as oil and gas industries, and construction materials due to the formation of a chromium oxide film on the metal surface [1–3]. But when the metals come into contact with mineral acids like hydrochloric acid, sulfuric acid, etc., especially during the prickling process, there will be material loss [4].

In order to prevent the material loss, the corrosive environment can be altered by adding the corrosion inhibitors. Most commonly organic compounds containing heteroatoms like O, N, S and P are used as protective agents. However, in recent years use of synthetic organic compounds are restricted because of environmental regulations [5–7]. In order to overcome this, research now is geared towards the use of green inhibitors. Plant products are reported to be excellent green inhibitors, as they are rich sources of tannins, alkaloids, flavonoids, etc. In addition, green inhibitors are biodegradable, environmentally benign, inexpensive and non-toxic [8, 9].

Sinapis alba (white mustard) has been the subject of diverse investigations in plant physiology. In the present investigation, we report the use of *Sinapis alba* as an eco-friendly corrosion inhibitor for the corrosion control of stainless steel in HCl acid medium, as a part of our research work with green corrosive inhibitors [11]. White mustard seeds are hard round seeds, usually around 1.0 to 1.5 mm in diameter, with a pale yellow colour [10]. The major active constituent present in *Sinapis alba* is reported to be Benzyl isothiocyanate. In addition to this, *Sinapis alba* also contains a large number of heterocyclic compounds like alkanoids, flavonoids etc.

EXPERIMENTAL

Material. Composition of stainless steel material composition is given below.

Preparation of test coupon. A cylindrical stainless steel rod with a diameter of 1 cm^2 and a height of 5 cm was prepared by moulding with cold setting acrylic resin. Polishing was done with different grades of emery papers with grit size of 200 to 1200 microns, and finally with a disc polisher using levigated alumina to obtain a mirror like surface. Then it was cleaned by double distilled water followed by acetone and dried for further use.

[1] The article is published in the original.

Table 1. Composition of the stainless steel specimens

Element	C	Si	Mn	Cr	Ni	Fe
Composition, %	0.0450	0.332	1.97	18.33	8.43	Balance

Preparation of medium. An acid stock solution was prepared by using 37% HCl and double distilled water. It was standardized by using previously standardized sodium hydroxide solution by volumetric titration. The standardized stock solution was diluted appropriately to get 0.5 M HCl solution.

Preparation of inhibitor solution. White mustard seeds were purchased from the commercial store. The seeds were washed with double distilled water and dried up to 1 weak without exposing directly to light. Then it was finely powdered using a domestic mixer grinder.

Sinapis alba seed extract (SASE) in an aqueous medium was prepared by taking 25 g of powdered white mustard seeds. It was refluxed in 500 mL distilled water up to 5 h and kept for overnight to settle down and filtered, then the filtrate was collected. After that, it was evaporated to complete dryness at 40°C in order to obtain a brown colour solid residue. The solid residue obtained was weighed and preserved in a desiccator for further use. It was then used for corrosion inhibition studies with concentration ranging from 0.005–0.01 g L^{-1}.

Electrochemical measurements. The electrochemical measurements of stainless steel in 0.5 M HCl were performed by using an electrochemical work station (CH600D-series, U.S. Model CH instrument with beta software). The electrochemical cell used was a conventional three electrode compartment Pyrex glass cell with platinum as counter electrode and a saturated calomel electrode (SCE) as reference electrode. Stainless steel was used as working electrode.

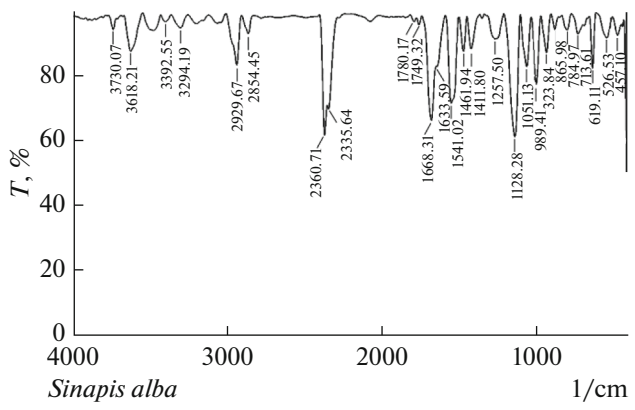

Fig. 1. IR spectrum of solid residue of SASE.

Potentiodynamic polarisation measurements. Potentiodynamic polarisation (PDP) studies were carried out for the stainless steel in 0.5 M HCl acid at different temperatures in the presence and absence of an inhibitor. A steady state open circuit potential was obtained at the end of 300 seconds period with respect to SCE. The potentiodynamic plots were obtained by polarising the stainless steel from –250 mV cathodically to +250 mV anodically, with respect to Open Circuit Potential (OCP) with a scan rate of 1 mV s^{-1}. With this corresponding corrosion current density (i_{corr}), corrosion potential (E_{corr}) and Tafel slope value were obtained.

Electrochemical impedance spectroscopy studies. Electrochemical impedance spectroscopy (EIS) studies for stainless steel were carried out in the frequency range from 10000 to 0.01 Hz by applying a small amplitude ac signal of 10 mV at the OCP. The procedure was repeated 3–4 times and best of the three agreeing values were repeated.

Surface studies. Scanning electron microscopy/energy dispersive X-ray (SEM/EDX) analysis: Surface morphology studies of stainless steel were carried out by immersing the specimen in 0.5 M HCl in the presence and absence of SASE for 2h using analytical scanning electron microscope (JEOL JSM-6380L) and elemental mapping was done by the EDX analysis.

RESULTS AND DISCUSSIONS

Fourier transforms infrared spectroscopy of SASE. Figure 1 is the Fourier transforms infrared **(**FTIR) spectrum of a solid residue of SASE, in which –N=C=S appears at a frequency of 2360 cm^{-1}. The fingerprint region at 2929 cm^{-1} is for the aromatic ring. The –C=C– stretching frequency appears at 1668 cm^{-1} and 1541 cm^{-1}, respectively. The phenolic –OH stretching appears at 3618 cm^{-1}. The FTIR spectrum confirms the presence of electron rich heteroatoms.

Electrochemical Measurements

PDP measurements. Figure 2 shows the PDP plots for stainless steel 0.5 M HCl with various concentrations of SASE along with the blank. Similar plots were obtained at different temperatures. Figure 2 shows that as the SASE inhibitor concentration increased, at 30°C there was a positive shift in the corrosion potential with respect to the blank. This indicates that the introduction of SASE as inhibitor controls the corrosion of stainless steel in an acid medium. A change in

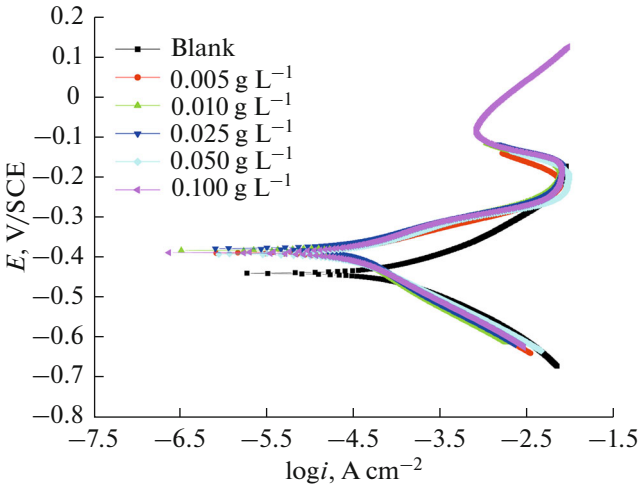

Fig. 2. PDP plots for corrosion of stainless steel in 0.5 M HCl containing different concentrations of SASE at 30°C.

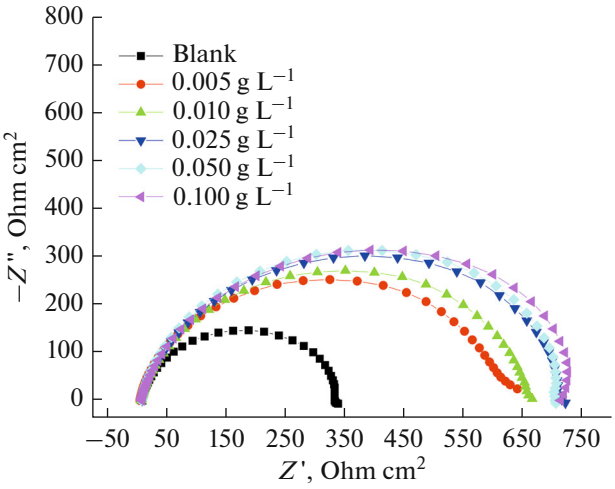

Fig. 3. Nyquist plot for corrosion of stainless steel in 0.5 M HCl containing different concentrations of SASE at 30°C.

the shape of the anodic slope is because of passivation observed in between −0.3 to −0.1 V. The cathodic polarization curves have linear behaviour and values of the cathodic slope ($-\beta_c$) are not varying significantly with an increase in the inhibitor concentration. This indicates that the hydrogen evolution is activation-controlled and the presence of an inhibitor did not alter the inhibition mechanism [12, 13]. According to the literature, if the displacement in the corrosion potential is over ±85 mV, against the corrosion potential of the uninhibited solution, the inhibitor can be considered to be of the cathodic or anodic type. However, the maximum displacement in this study was not over 85 mV, which indicates that our inhibitor is a mixed-type inhibitor [14].

The PDP for stainless steel in an acid medium in the presence and absence of SASE are obtained from this study. The corrosion rate and % efficiency of SASE were calculated using equations 1 and 2, respectively.

$$CR\left(\text{mmy}^{-1}\right) = \frac{3270 \times M \times i_{\text{corr}}}{\rho \times z}, \qquad (1)$$

where 3270 is a constant that defines the unit of corrosion rate, i_{corr} is the corrosion current density in A cm^{-2}, ρ is the density of the corroding material (g cm^{-3}), M is the atomic mass of the metal and Z is the number of electrons transferred per atom.

$$IE\,(\%) = \frac{i_{\text{corr}} - i_{\text{corr(inh)}}}{i_{\text{corr}}} \times 100, \qquad (2)$$

where i_{corr} and $i_{\text{corr (inh)}}$ are the corrosion current densities in the absence and presence of the inhibitor, respectively. Table 2 shows PDP values for stainless steel in the presence and absence of SASE at different temperatures.

As the inhibitor concentration increased, the corrosion current density decreased. It is evident that the percentage of efficiency of the inhibitor increased with an increase in the concentration of SASE and also with an increase in the temperature because of adsorption of inhibitor on the metal surface. The maximum inhibition efficiency of 88% was observed at 45°C, for a higher concentration of the inhibitor of 0.1 g L^{-1}. This indicates that SASE gets adsorbed over the metal surface at a very high temperature and thus protects the stainless steel from undergoing the corrosion.

EIS studies. Figure 3 shows the Nyquist plot of stainless steel in 0.5 M HCl with different concentrations of SASE; the same plots are obtained for all temperatures. The semicircle in this plot indicates a charge transfer controlled process [15]; the diameter of the semicircle increases with an increase in the inhibitor concentration, which indicates that the inhibitor protects the metal from corrosion. The Nyquist plots with a depressed capacitive loop at a high-frequency range demonstrate the surface roughness, inhomogeneity of the solid surface and also the adsorption of the inhibitor on the metal surface [16]. The high frequency capacitive loop could be assigned to the charge transfer of the corrosion process and to the formation of an oxide layer [17].

The impedance data were simulated to get an appropriate equivalent circuit using 3.21 version of Zimpwin software, which is presented in Fig. 4a,b, respectively.

The equivalent circuit consists of a solution resistance (R_S), a charge transfer resistance (R_{ct}), an inductive resistance (R_L) and an inductive element (L). It also consists of a constant phase element (CPE, Q),

Table 2. Results of PDP studies for corrosion of stainless steel in 0.5 M HCl containing various concentrations of SASE at different temperatures

Temp., K	SASE, g L^{-1}	E_{corr}, mV vsSCE	$i_{corr} \times 10^{-5}$, A cm^{-2}	β_a, mV dec^{-1}	$-\beta_c$, mV dec^{-1}	CR, mmy^{-1}	IE, %
303	Blank	–440	7.385	1023	1031	16.61	–
	0.005	–390	2.381	1938	827	5.35	67.88
	0.01	–383	2.173	1987	775	4.88	70.57
	0.025	–379	1.937	2238	781	4.35	73.77
	0.05	–393	1.784	2277	987	4.01	75.84
	0.1	–389	1.662	2393	902	3.73	77.49
308	Blank	–441	10.51	1073	1053	23.63	–
	0.005	–365	2.827	1842	783	6.35	73.10
	0.01	–408	2.580	2029	979	5.80	75.45
	0.025	–411	2.402	2230	986	5.40	77.14
	0.05	–380	2.039	2664	903	4.58	80.59
	0.1	–392	1.905	2849	1029	4.28	81.87
313	Blank	–444	14.40	1104	1080	32.39	–
	0.005	–402	3.463	2114	1038	7.78	75.95
	0.01	–373	2.793	2129	806	6.01	80.60
	0.025	–378	2.315	2428	885	4.40	83.92
	0.05	–388	2.064	2734	985	4.28	85.66
	0.1	–392	1.970	2912	1054	4.07	86.31
318	Blank	–442	15.49	1157	1047	34.83	–
	0.005	–406	3.575	1747	1040	8.04	76.92
	0.01	–396	2.676	2511	1018	6.28	82.72
	0.025	–391	1.959	2608	1072	5.20	87.35
	0.05	–392	1.905	2849	1029	4.64	87.70
	0.1	–393	1.784	2277	9879	4.01	88.48

which is parallel to the series of the capacitances C_1 and C_2, while the resistors R_1, R_2, R_L and R_{ct} and R_L are parallel to the L inductor.

A double layer capacitance (C_{dl}) and a polarization resistance (R_p) can be obtained by using equations (3) and (4), respectively,

$$C_{dl} = C_1 + C_2, \quad (3)$$

$$R_p = R_1 + R_2 + R_L + R_{ct}. \quad (4)$$

R_p is inversely proportional to the corrosion current and it can be used to calculate the percentage inhibition efficiency using relation (5).

$$IE(\%) = \frac{R_{p.corr(inh)} - R_{p.corr}}{R_{p.corr(inh)}} \times 100, \quad (5)$$

where $R_{p.corr(inh)}$ and $R_{p.corr}$ are the polarization resistances in the presence and absence of the inhibitor.

Table 3 shows the results obtained via the EIS technique. The double layer capacity was calculated using equation (6).

$$C_{dl} = Q_{dl} \times (2\pi f_{max})^{(a-1)}. \quad (6)$$

As observed in Table 3, R_p values increase with an increase of the concentration of SASE, while C_{dl} values decreased because of an increase in the thickness of the electrical double layer in between the metal and the solution interface [18]. The results of PDP are in good agreement with those of EIS.

Effect of temperature. To understand the adsorption behaviour of SASE on stainless steel, the effect of temperature was studied and the activation parameters

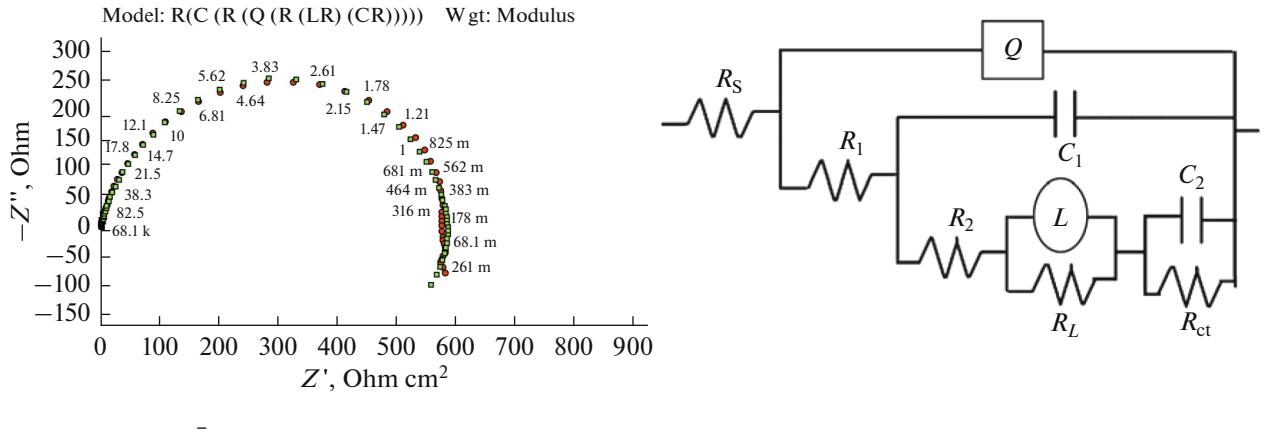

Fig. 4. (a) Simulated Impedance data for stainless steel corrosion in 0.5 M HCl at 35°C; (b) equivalent circuit of nine elements.

such as the energy of activation (E_a), the enthalpy (ΔH_a) and the entropy of activation (ΔS_a) values were obtained. The E_a can be calculated from the Arrhenius law equation (7).

$$\ln(CR) = B - \frac{E_a}{RT}, \quad (7)$$

where B is the Arrhenius constant which depends upon the metal type; R is equal to 8.314 JK^{-1} mol^{-1}, T is the absolute temperature. Figure 5 shows the Arrhenius plot of stainless steel plotted against ln(CR) vs $1/T$. From the slope of the straight line, the E_a was calculated.

The transition state equation (8) was used to calculate the enthalpy (ΔH_a) and the entropy of activation (ΔS_a) for the dissolution of the metal

$$CR = \frac{RT}{Nh}\exp\left(\frac{\Delta S_a}{R}\right)\exp\left(-\frac{\Delta H_a}{RT}\right), \quad (8)$$

where h is Plank's constant (6.626×10^{-34} Js), N is Avogadro's number (6.023×10^{-23} mol^{-1}).

The plot of ln(CR/T) vs $1/T$ was linear. The slope of this straight line gave the value of the enthalpy of activation while the intercept gave the value of the entropy of activation. Figure 6 is the plot of ln(CR/T) verses $1/T$ for stainless steel in various concentrations of SASE in 0.5 M HCl. The data for the activation parameters for the corrosion of stainless steel in 0.5 M HCl containing different concentrations of SASE are given in Table 4.

The E_a values of the stainless steel in the presence of SASE are lower than those in the absence of the inhibitor. This decrease of the E_a values of the inhibited solution indicates that there is chemical adsorption of SASE, as inhibitor, on the surface of the stainless steel, and then they attain equilibrium at higher temperatures [19, 20]. The inhibitor molecule gets chemically adsorbed on the metal surface and decreases the electrochemical corrosion process [21–23].

The E_a values of the stainless steel in the presence of SASE are lower than those in the absence of the

Table 3. Impedance values obtained for corrosion of stainless steel in 0.5 M HCl containing various concentrations of SASE at different temperatures

Temp, K	SASE, g L^{-1}	$C_{dl} \times 10^{-5}$, F cm^{-2}	R_p, Ω cm^2	IE (%)
303	Blank	11.72	287	–
	0.005	10.51	660	56.5
	0.01	9.24	724	60.35
	0.025	8.55	743	61.37
	0.05	8.43	747	61.57
	0.1	6.93	794	63.85
308	Blank	16.90	195	–
	0.005	14.80	586	66.72
	0.01	11.16	560	65.17
	0.025	10.64	563	65.36
	0.05	5.95	589	66.89
	0.1	5.26	598	67.39
313	Blank	18.12	138	–
	0.005	11.70	398	75.32
	0.01	8.29	530	73.93
	0.025	7.67	556	75.17
	0.05	6.82	566	75.61
	0.1	5.42	567	75.66
318	Blank	22.61	127	–
	0.005	12.34	436	70.89
	0.01	9.95	460	72.39
	0.025	8.38	589	78.43
	0.05	6.93	604	78.97
	0.1	6.08	747	82.99

Table 4. Activation parameter for the corrosion of stainless steel in 0.5 M HCl containing different concentrations of SASE

SASE, gL^{-1}	E_a, kJ mol^{-1}	ΔH_a, kJ mol^{-1}	ΔS_a, J mol^{-1} K^{-1}
Blank	39.061	36.589	−189.51
0.005	21.991	19.519	−197.46
0.01	12.084	9.612	−201.47
0.025	4.634	2.162	−204.53
0.05	5.486	3.014	−204.29
0.1	6.969	4.497	−203.78

inhibitor. This decrease of the E_a values of the inhibited solution indicates that there is chemical adsorption of SASE, as inhibitor, on the surface of the stainless steel, and then they attain equilibrium at higher temperatures [19, 20]. The inhibitor molecule gets chemically adsorbed on the metal surface and decreases the electrochemical corrosion process [21–23]. The positive sign of ΔH_a indicates that there is the endothermic process of stainless steel metal dissolution [24]. The entropy of activation (ΔS_a) data are negative, which indicates decrease in the disorderness ongoing from reactant towards the formation of activated complex [25, 26].

Adsorption isotherm. The data of the surface coverage obtained from the PDP studies were applied for various types of adsorption isotherms such as the Langmuir, Freundlich, Temkin and Frumkin ones, being best fitted with the Langmuir adsorption isotherm that can be related by relationship (9)

$$\frac{C}{\theta} = \frac{1}{K} + C, \tag{9}$$

where, K is the adsorption/desorption equilibrium constant (L mol^{-1}) and C is the concentration of inhibitor molecules. The fraction of the surface coverage θ is given by equation (10)

$$\theta = \frac{IE(\%)}{100}. \tag{10}$$

Figure 7 represents the Langmuir adsorption isotherm plot for stainless steel. The plot of $\frac{c}{\theta}$ versus C gave a straight line from which the intercept values were obtained. The isotherm slopes showed deviation from the value of unity as would be expected for the ideal Langmuir adsorption isotherm equation. This deviation may be because of the interaction among the adsorbed inhibitor on the metal surface. The standard free energy of adsorption $\left(\Delta G^0_{ads}\right)$ can be calculated by using the values of K, which is related by equation (11).

$$K = \frac{1}{55.55}\exp\left(-\Delta G^0_{ads}/RT\right), \tag{11}$$

where R is the universal gas constant, T is the absolute temperature; the value 55.55 in the above equation is the concentration of water in the solution in mol^{-1}.

The values of the standard enthalpy of adsorption $\left(\Delta H^0_{ads}\right)$ and the standard entropy of adsorption $\left(\Delta S^0_{ads}\right)$ were obtained by plotting ΔG^0_{ads} vs T in Fig. 8 that shows a linear plot. From the slope of the straight

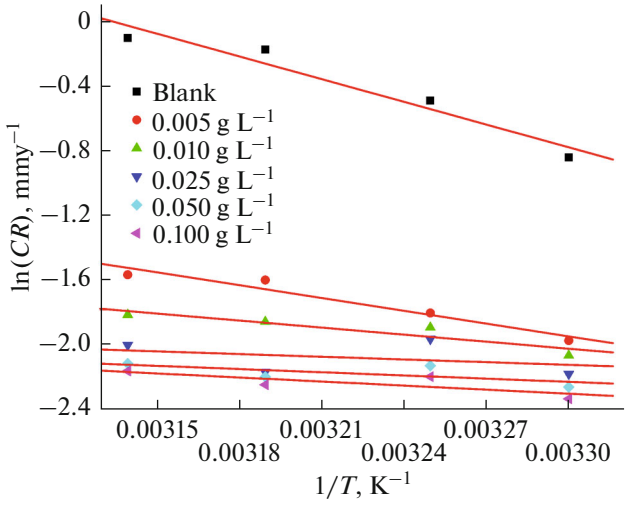

Fig. 5. Arrhenius plots for the corrosion of stainless steel in 0.5 M HCl at different concentrations of SASE.

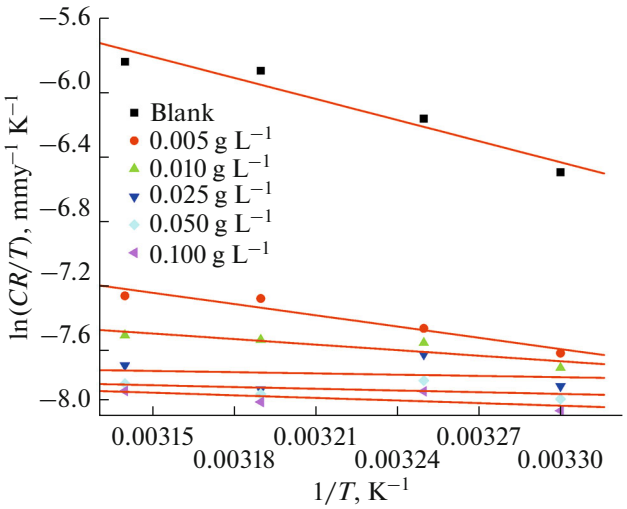

Fig. 6. Plots of ln(CR/T) vs $1/T$ for the corrosion of stainless steel in 0.5 M HCl containing different concentrations of SASE.

line a value of ΔS^0_{ads} and from the intercept of the straight line values of ΔH^0_{ads}, were calculated by using the Gibbs Helmholtz equation (12).

$$\Delta G^0_{ads} = \Delta H^0_{ads} - T\Delta S^0_{ads}. \quad (12)$$

When ΔG^0_{ads} value is up to –20 kJ mol^{-1} then we considered that there is an electrostatic interaction between the negatively charged metal surface and the protonated inhibitor molecule, i.e. there is physisorption. When its value is negative and less than –40 kJ mol^{-1}, then we considered that there is the sharing of electrons or their transfer from the inhibitor molecule to the surface of the metal through coordinate bond formation, i.e. there is chemisorption [26].

The negative value of ΔG^0_{ads} in Table 5 implies the spontaneous adsorption of the inhibitor onto the surface of the stainless steel. The ΔG^0_{ads} values increased with an increase in temperature, which implies that the adsorption of the inhibitor on the surface of the stainless steel is mainly via chemisorption [27]. According to the just reported literature, if the values are less than –40 kJ mol^{-1}, then adsorption may be physical adsorption, and if it is in between –40 and –100 kJ mol^{-1}, then it is considered as chemical adsorption of the inhibitor. But the positive value of ΔH^0_{ads} clearly confirms the chemical adsorption of SAES on the surface of the stainless steel metal [27].

Mechanism of corrosion. Based on the adsorption phenomenon, the corrosion inhibition of metals in acidic solution can be described. In the present study, the adsorption of SASE on stainless steel can be attributed to either sharing of electrons between the hetero atoms and iron or to the π-electron interaction between the aromatic ring of the SASE and the metal surface [28]. SASE is rich in hetero atoms, with an active constituent of SASE—benzyl isothiocyanate, whose structure is as shown in Fig. 9.

The mechanism of inhibition can be predicted from the knowledge of the interaction between the inhibitor molecules and the surface of the metal. In acid solutions, the mechanism of dissolution of stainless steel takes place as follows.

In the anodic region:

$$Fe + Cl^- \rightarrow FeCl^-_{(ads)}, \quad (13)$$

$$FeCl^-_{(ads)} \leftrightarrow FeCl_{(ads)} + e^-, \quad (14)$$

$$FeCl_{(ads)} \leftrightarrow (FeCl)^+ + e^-, \quad (15)$$

$$(FeCl)^+ \leftrightarrow Fe^{2+} + Cl^-. \quad (16)$$

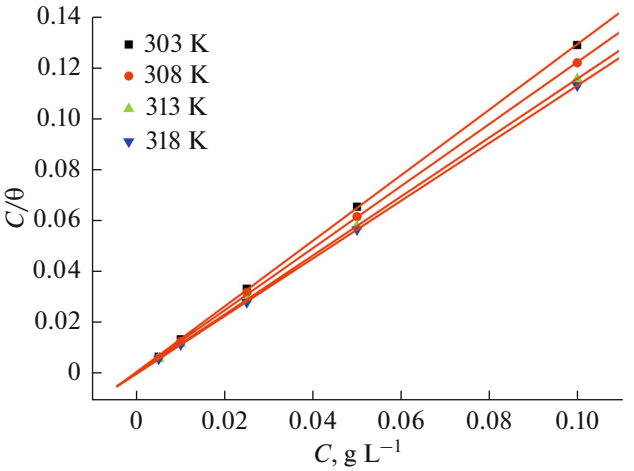

Fig. 7. Langmuir adsorption isotherm for adsorption of SASE on stainless steel in 0.5 M HCl at different temperatures.

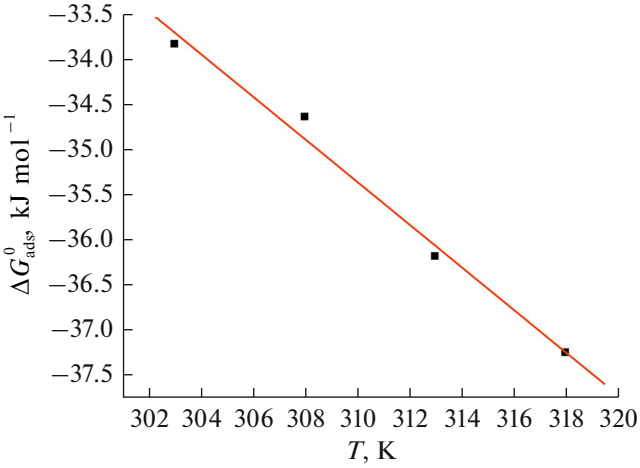

Fig. 8. Plot of ΔG^0_{ads} vs. T.

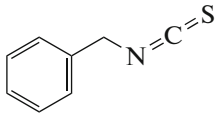

Fig. 9. Structure of benzyl isothiocyanate.

The major cathodic reaction is evolution of hydrogen gas according to the following steps:

$$FeH^+_{(ads)} + e^- \leftrightarrow FeH_{(ads)}, \quad (17)$$

Table 5. Thermodynamic parameters of stainless steel in 0.5 M HCl

Temp., K	ΔG^0_{ads}, kJ mol^{-1}	ΔH^0_{ads}, kJ mol^{-1}	ΔS^0_{ads}, kJ mol^{-1} K^{-1}
303	–33.81	38.06	0.236
308	–34.62		
313	–36.17		
318	–37.24		

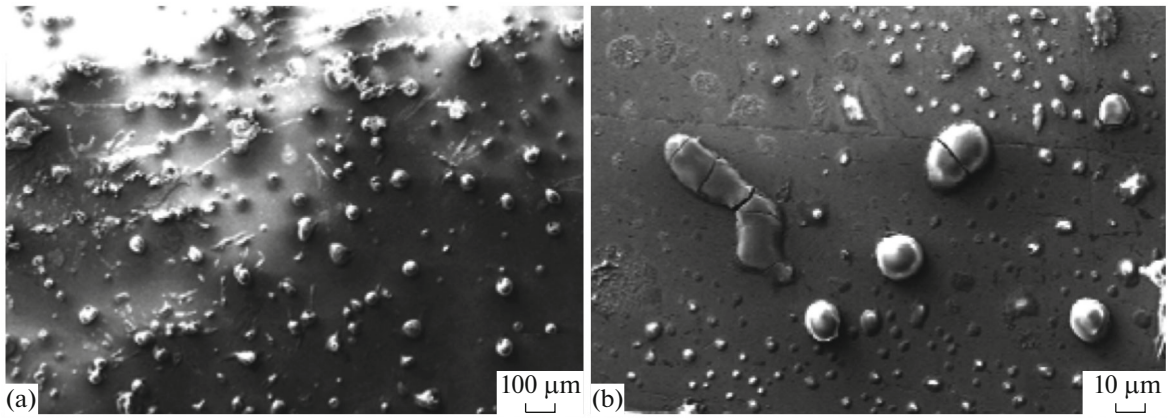

Fig. 10. SEM image: (a) SS + 0.5 M HCl; (b) SS + 0.5 M HCl + 0.1 g L^{-1} SASE.

$$FeH_{(ads)} + e^- \leftrightarrow Fe + H_2. \quad (18)$$

The adsorption of the inhibitor molecule is often a displacement reaction [29] involving the removal of the adsorbed water molecules from the metal surface as shown in the following:

$$Inh_{(solution)} + nH_2O_{(Adsorption)} \rightarrow Inh_{(Adsorption)} + nH_2O_{(solution)}. \quad (19)$$

The vacant 3*d* orbital of iron can form a coordinate type of a bond with the inhibitor due to the interaction of *p*-electron clouds of aromatic rings as well as unshared electron pairs on the nitrogen or sulphur atoms of the benzyl isothiocyanate leading to predominant chemisorption and preventing the stainless steel from undergoing corrosion in acid medium.

SEM and EDX studies. SEM investigation was carried out to differentiate between the surface morphology of the metal surface after its immersion in 0.5 M hydrochloric acid for 2 h in the absence and presence of SASE. Figure 10a shows the cracks and rough surface of the stainless steel due to the corrosive action of 0.5 M hydrochloric acid. Figure 10b shows the smooth sample surface without any visible corrosion attack or pits in the presence of SASE. This confirms the adsorption of SASE on the stainless steel surface through the formation of a protective film of the studied inhibitor on the metal surface.

Elemental mapping was done with the EDX analysis. The results are given in Table 6.

When the specimen was immersed in the corrosive medium, there was a peak corresponding to chlorine (4.60%). This indicates the interaction of the medium with the material and hence the corrosion of stainless steel, which is evident due to a decrease in the concentration of Cr (14.45%) and Ni (6.64%). After the addition of the inhibitor, the content of chlorine decreased (2.77%). An increase in the carbon content (14.1%) confirms the adsorption of the inhibitor on the metal surface.

CONCLUSIONS

—The inhibition efficiency of SASE increases with an increase in the concentration of the studied inhibitor and with an increase in temperature.

—SASE acted as a mixed type inhibitor for stainless steel in 0.5 M HCl medium.

—SASE got chemically adsorbed on the metal surface and obeyed the Langmuir adsorption isotherm.

Table 6. EDX data obtained before and after corrosion inhibition of stainless steel surface is with SASE

Elements	% Composition								
	C	Si	Cl	Cr	Mn	Fe	O	Ni	Cu
Freshly polished SS	2.62	0.41	–	18.03	1.89	68.94	–	8.11	0.57
SS in 0.5 M HCl	–	0.30	4.60	14.45	1.63	54.45	12.66	6.64	0.55
SS in 0.5 M HCl + 0.1 g L^{-1} SASE	14.1	0.56	2.77	15.65	1.74	59.63	7.34	7.19	–

—The surface studies via SEM/EDX supported the existence of the adsorption of the inhibitor on metal surface.

—The results obtained by PDP and EIS were in good agreement with each other.

—SASE emerged as a potential green corrosion inhibitor with its maximum efficiency of 88.48% at 45°C for 0.1 g L^{-1}.

REFERENCES

1. Ovri, J.E.O., *Niger. Corros. J.*, 1998, vol. 1, pp. 65–72.
2. Tao, Z., Zhang, S., Li, W., and Hou, B., *Corros. Sci.*, 2009, vol. 51, pp. 2588–2595.
3. Singh, A.K. and Quraishi, M.A., *Int. J. Electrochem. Sci.*, 2012, vol. 7, pp. 3222–3241.
4. Singh, D.D.N., Singh, T.B., and Gaur, B., *Corros. Sci.*, 1995, vol. 37, pp. 1005–1019.
5. Wang, L., *Corros. Sci.*, 2006, vol. 48, pp. 608–616.
6. Noor, E., *Corros. Sci.*, 2005, vol. 47, pp. 33–55.
7. Sanyal, B., *Prog. Org. Coat.*, 1981, vol. 9, pp. 165–236.
8. Obot, I.B. and Obi-Egbedi, N.O., *Int. J. Electrochem. Sci.*, 2009, vol. 4, pp. 1277–1288.
9. Obot, I.B. and Obi-Egbedi, N.O., *Port. Electrochim. Acta*, 2009, vol. 27, pp. 517–524.
10. Gupta, V., *Indian J. Pharm.*, 1994, vol. 26, pp. 1–12.
11. Deepa, P. and Padmalatha, R., *J. Environ. Chem. Eng.*, 2013, vol. 1, pp. 676–683.
12. El Kadher, A., El-Warraky, J.M., and Abd-El Aziz, A.M., *Br. Corros. J.*, 1998, vol. 33, pp. 139–144.
13. Li, W.H., He, Q., Zhang, S., Pei, C.L., et al., *J. Appl. Electrochem.*, 2008, vol. 38, pp. 289–295.
14. Shahin, M., Bilgic, S., and Yilmaz, H., *Appl. Surf. Sci.*, 2003, vol. 195, pp. 1–7.
15. Li, W.H., He, Q., Zhang, S., Pei, C.L., et al., *J. Appl. Electrochem.*, 2008, vol. 38, pp. 289–295.
16. Mansfeld, F., Lin, S., Kim, K., and Shih, H., *Corros. Sci.*, 1987, vol. 27, pp. 997–1000.
17. Poornima, T., Jagannatha, N., and Nithyananda, A.S., *J. Appl. Electrochem.*, 2011, vol. 41, pp. 223–233.
18. Poornima, T., Jagannatha, N., and Nithyananda, A.S., *Port. Electrochim. Acta*, 2010, vol. 28, pp. 173–188.
19. Ameer, M.A., Khamis, E., and Al-Senani, G., *J. Appl. Electrochem.*, 2002, vol. 32, pp. 149–156.
20. Osman, M.M., El-Ghazawy, R.A., and Al-Sabagh, A.M., *Mater. Chem. Phys.*, 2003, vol. 80, pp. 55–62.
21. Oguzie, E.E., Njoku, V.O., Enenebeaku, C.K., Akalezi, C.O., et al., *Corros. Sci.*, 2008, vol. 50, p. 3481.
22. Ashassi-Sorkhabi, H., Shaabani, B., and Seifzadeh, D., *Appl. Surf. Sci.*, 2005, vol. 239, pp. 154–164.
23. Bouklah, M., Hammouti, B., Lagrenee, M., and Bentiss, F., *Corros. Sci.*, 2006, vol. 48, pp. 2831–2842.
24. Sahin, M., Bilgic, S., and Yilmaz, H., *Appl. Surf. Sci.*, 2002, vol. 195, pp. 1–7.
25. Soltani, N., Behpour, M., Ghoreishi, S.M., and Naeimi, H., *Corros. Sci.*, 2010, vol. 52, pp. 1351–1361.
26. Bentiss, F., Traisnel, M., and Lagrenee, M., *J. Appl. Electrochem.*, 2001, vol. 31, pp. 41–48.
27. Quraishi, M.A., Rawat, J., and Ajmal, M., *J. Appl. Electrochem.*, 2000, vol. 30, pp. 745–751.
28. Khaled, K.F. and Hackerman, N., *Electrochim. Acta*, 2003, vol. 48, pp. 2715–2723.
29. Singh, A.K. and Quraishi, M.A., *Corros. Sci.*, 2010, vol. 52, pp. 152–160.